Trim Simulations of Thin Film Resistors by the Boundary Element Method (BEM)

Klaus Schimmanz
Chair of Numerical and Applied Mathematics
TU Cottbus, Germany
Email: kschimm@vitr.org

Arnulf Kost
Chair of Fundamentals in Electrical Engineering and Computational Electromagnetics
TU Cottbus, Germany
Email: Arnulf.Kost@aet.tu-cottbus.de

***Abstract*— The reliability of resistors in the modern hybrid integrated circuit production becomes more and more important. This paper discusses a method to evaluate post-trim drift behavior of laser trimmed thin film resistors. Based on numerical flux field computations a dynamic post-trim drift model is deduced and it will be shown how the Boundary Element Method (BEM) is used to simulate such processes.**

I. Introduction

High precision resistors are responsible for functionality, capability and reliability of modern hybrid IC's. In practice high precision resistors are difficult to manufacture. In difference to monolithic diffusion resistors planar thin film resistors on silicon chips are trimable and that's why they are frequently applied to meet precise resistance specifications. Furthermore, film resistors on silicon chips are mainly used to compensate various manufacture process variations of other circuit components. Today, such singular resistance adjustments are performed by laser trimmings on wafer level. This has become the most popular method of individually tailoring each die on a silicon wafer to meet precise resistor specifications. The used lasers operate in pulsed mode due to energy reasons. When the laser beam travels rapidly across the resistor being trimmed each pulse vaporizes a small spot of film material and the individual pulses overlap creating a close, and clean cut line into the resistor. Such shape changes always elevate the resistance, pulse by pulse - dependent on the concrete trim path figure.

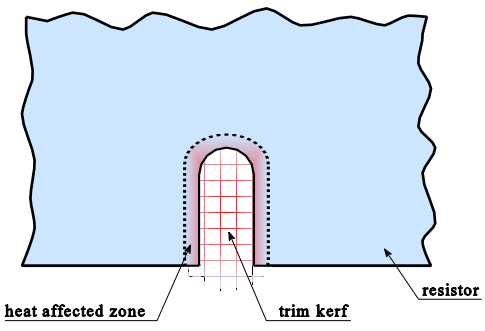

Fig. 1. Heat-Affected-Zone at trim kerf edge

The laser process itself has an impact on the long term stability of each trimmed resistor. This disadvantage is caused by thermal and mechanical shock each laser pulse induces into the material next to any trim kerf edge. The region is called *Heat Affected Zone (HAZ)* and it shows altered, unstable properties (see Fig. 1). This effect cannot be avoided completely. Relaxation processes of that zone are responsible for the additional resistance drift of trimmed resistors. Thus, it is essential to know for resistor layout design how trimmed resistors behave, if there is a premium on high accuracy and stability. Because of the high costs involved in the trim process, there is the desire to evaluate trim and post-trim drift resistance changes, rather by carrying out of simulations than by real world experiments. Thus, the following sections introduce an approach to model such effects numerically, whereby the main focus here is on drift issues. For trim simulation usage in resistor shape and for trim path layout designs see [1].

II. Post-Trim Drift Model

The laser trim process is changing the resistor geometry by a trim strategy which always leaves an unstable zone next to each cut path as mentioned above. The material being vaporized very quickly provokes a short, intense pressure blast, what compresses the remaining rim zone material along the cut pathway mechanically. Since the laser intensity profile is approximately Gaussian in shape, the edges of the kerf are inadvertently heated while the center of the kerf is being vaporized. This cannot be fixed by simply raising laser power since the HAZ would just move over forming a wider cut. The edge material gets cracked and anneals amorphous and chaotic. Thus, the sheet material will have another electrical characteristics than somewhere else. But it will be still a part of the current carrying path. The concrete HAZ conductivity is usually unknown as well as its geometry. The amorphous, chaotic zone character destabilizes the resistor in use because of a lot of microscopic acute re-entry corners. At these locations the power density can be extreme, if a current flow is present. That means there will be an intense energy conversion into heat what will release the 'frozen' mechanical HAZ strains and finally round down these re-entry corners. Therefore, the electrical zone characteristic will alter again and a resistance post-trim drift appears. But the whole HAZ becomes more and more relaxed and the drift process continues to slow down with time.

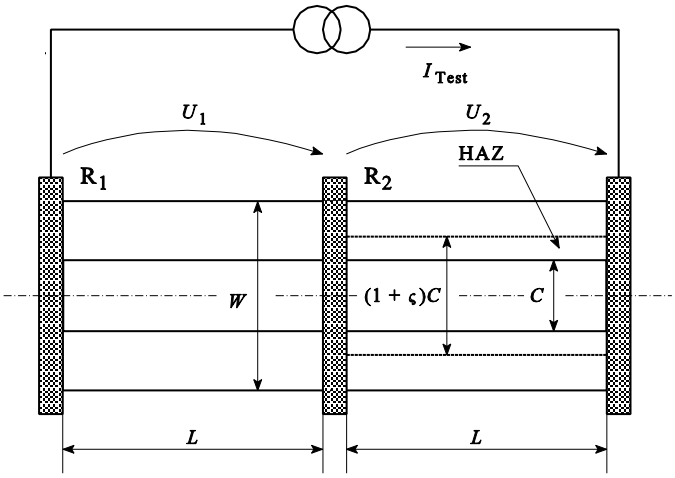

Fig. 2. Test geometry for characterizing trim induced drift due to the heat affected zone (C: trim laser kerf width)

In practice it can be observed that elevated temperatures tend to accelerate the drift but basically similar results occur. A simple model which adequately accounts for this laser induced drift is to assume that the laser cut widens and eventually stabilizes with time. To characterize the maximum HAZ drift of a given film system and laser combination is to fabricate a pair of resistors as shown in Fig. 2 whereby only the right center cut is made by the trim laser. During a life test the ratio of resistor voltage drops is measured while being excited with a constant current source as shown. After sufficient stabilization the kerf HAZ-fraction ς can be calculated as follows:

$$\varsigma = \left(1 - \frac{U_1}{U_2}\right)\left(\frac{W}{C} - 1\right) \tag{1}$$

This kerf widening is a virtual one, of course, and invisible. Using the HAZ-fraction parameter ς for different cut figures in field computations gives the designer a criterion to chose the one with the lowest possible drift. This leads to maximum HAZ-index model as introduced in [1]. In general it can be shown that the local domain scaling at border lines is an equivalent for other conductivities of the heat affected zone (see [1]). Using this in dependence on local zone temperature delivers further a dynamical post-trim drift model. It has been observed that the drift velocity decreases exponentially with time. Using the geometrical equivalence this can be interpreted by a node movement of the HAZ-contour and leads to the formulation:

$$\frac{\mathrm{d}m}{\mathrm{d}t} = v_0 e^{-\alpha Q(t) t}\ ,\ \alpha, Q(t) > 0,\ \alpha = const. \tag{2}$$

where Q expresses the present energy density excited by the current flow which is an equivalent expression of heat induction, α is a constant factor describing the energy efficiency of relaxation and t is the simulation time. The maximum distance each node can go is limited by the HAZ-fraction parameter as $m_\infty = \varsigma C/2$ and thus, the initial velocity has to be $v_0 = \alpha Q m_\infty$. Numerical algorithms like BEM are splitting the border into short segments and defines nodes at the boundary. The dynamical post-trim drift model couples each boundary node i of trim kerfs boundary with a close, interior sample point where the local power density ϱ_i will be taken from (Fig. 3). Discrete integration of ϱ_i over time under respect of an energy loss ν gives the energy density Q_i at each node i. Finally the integration of (2) leads to the necessary node moving function:

$$m_i(t_j) = \begin{cases} \tilde{m} := m_\infty \left(1 - \mathrm{e}^{-\alpha t_j (Q_i(t_j) + Q_T)}\right) & , \tilde{m} > m_i(t_{j-1}) \\ m_i(t_{j-1}) & , \text{otherwise} \end{cases} \tag{3}$$

$$Q_i(t_j) = \nu(\Delta t)\, Q_i(t_{j-1}) + \varrho_i(t_j)\Delta t$$

where m_∞ is the maximum node move range, t_j the discrete time, ν the constant energy loss factor and Q_T an external energy density. The iterative use of (3) is changing domains geometry for each time step and it produces a view graph of post-trim drift versus time by resistance computation for each t_j.

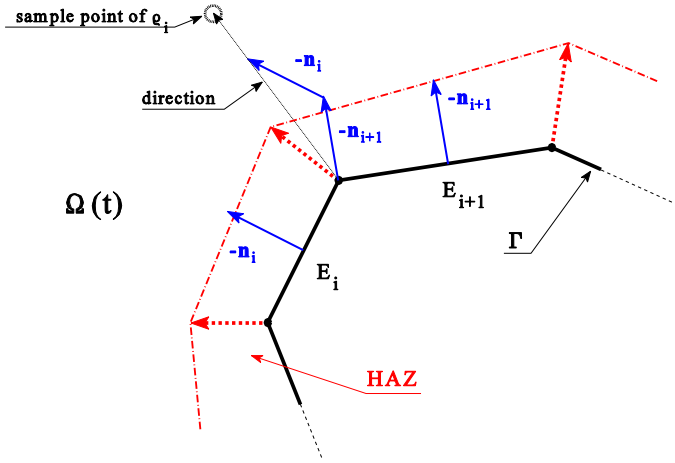

Fig. 3. Movement (dashed arrows) and power density sampling of a HAZ-boundary node ($\mathbf{n}$: outward vector unit normal; E_i: Element i; $\Omega(t)$: domain at time t; Γ: domains contour)

III. Resistance Computation and Method Selection

The resistance of a film resistor is determined by its geometry and by the electrical property of the used film material. The effect of laser trimmings be due to changing the geometry by vaporizing the film partially, as mentioned above, which increases its resistance. For the pure ohmic resistance a stationary current flux field through the domain Ω is to consider. The resulting stationary potential field φ has to satisfy the Laplacian partial differential equation under the assumption that the used material within the domain is a homogeneous, linear, and isotropic one. To excite a stationary flux field within the resistor a constant potential difference between the two terminals is necessary. In the example of Fig. 4 the terminals are at the vertical sides of the resistor. Because the objective for film resistors is to produce a constant

sheet thickness z and having all over the same conductivity κ, the whole problem is treatable as a 2-dimensional one. Thus, the domain has exact two different Dirichlet boundaries, Γ_1 and Γ_3 - distinct from each other - and all other edges are homogeneous Neumann ones.

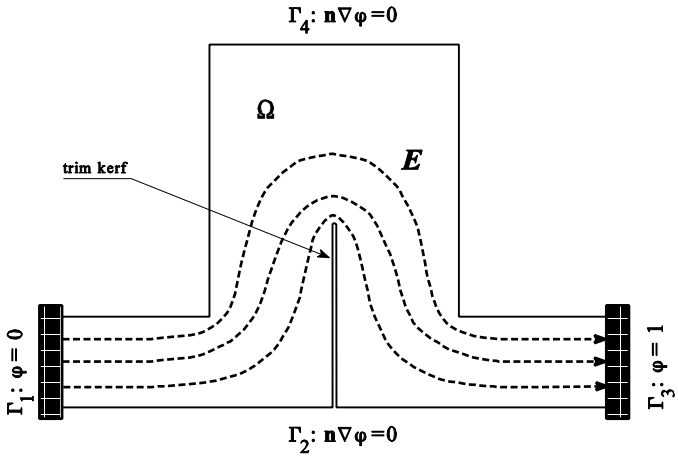

Fig. 4. Top-hat resistor shape with central trim cut and electrical field (Γ_1, Γ_3: terminals; Γ_2, Γ_4: insulated edges)

Ohm's law says that the resistance is the quotient of voltage by total current through the structure. The voltage is given by the used potential difference of the Dirichlet edges $\varphi(\Gamma_3) - \varphi(\Gamma_1)$ and the structur's total current can be obtained by integration of the normal current density $\vec{n}\nabla\varphi$ along one Dirichlet boundary multiplied by the conductivity κ and the sheet thickness z. All together it gives for the film resistance R:

$$R = \left| \frac{\varphi(\Gamma_3) - \varphi(\Gamma_1)}{\kappa z \int_{\Gamma_3} \frac{\partial\varphi(x,y)}{\partial n} \, \mathrm{d}\Gamma} \right| \text{, where } \Delta\varphi(x,y) = 0 \text{ on } \Omega \quad (4)$$

and $\vec{n}$ is the outward unit normal on Γ (Fig. 4).

For almost all outlines used here, Laplacian equation is not solvable analytically. But several numerical methods are applicable for this, like Finite Element Method (FEM) or Boundary Element Method (BEM). The BEM, however, proves to be beneficial for this application. First of all, the problem here is a homogeneous and linear one, where no volume discretization is necessary and so it is dedicated for the BEM. Hence, the mesh generation is a one-dimensional problem only. Refinement issues can remain in user's responsibility because insufficient results become pretty soon obvious during the simulation process. Therefore adaptional refinement cycles can be avoided and thus, preset and equidistant elements are useable. Second of all, values of the directed derivatives needed by the integration in (4) are already present in the collocation points and no further effort is necessary for that. This simplifies and speeds up the integration procedure. Third of all, the BEM minimizes the residuum on the boundary by design. This is not the case by the FEM. Hence, the BEM provides more consistent results than the FEM. Furthermore, the BEM shows a better treatment of boundary singularities

TABLE I

EXEMPLARY COMPARISON OF DIFFERENT NUMERICAL METHODS FOR RESISTANCE COMPUTATIONS OF A 4:1 BAR RESISTOR WITH 70% P-CUT AT LENGTH FOURTH (COMPUTED ON 200MHZ PENTIUM; MEASURED RESISTANCE $5.1\Omega \pm 0.01\Omega$)

Method	FEM	BEM
Nodes / Elements	1,349 Nodes 2,586 Elements	209 Nodes 209 Elements
Net type	linear, triangles	constant, straight
Resistance	5.0725 Ω	5.0904 Ω
Lin. equation solver	Cholesky	Gaussian column pivot.
Net adaptions	10	-
Memory consumption	690,524 Bytes	438,900 Bytes
Global error index	$3.8 \cdot 10^{-3}$	$1.5 \cdot 10^{-4}$
Time consumption	46s	9s

than the FEM. All this leads to significant time savings for computation (together up to a factor of 5). In addition, BEM's memory usage is smaller than for FEM in the same case and for similar results (relation often about 2:3). The same is to say about the program code complexity (relation is greater than 1:6 for number of source code lines). For further details the reader is referred to [1], [2]. Table I presents a numerical example. The resistance can be computed in two ways by (4): once by integration along Γ_1 and a second time by integration along the contour Γ_3. The global error index is the absolute difference of these both resistances.

IV. POWER DENSITY DISTRIBUTION

Sheet power density distribution is one of the driving factors for layout sizing during resistor design. Minimizing of resistor real estate usage is a prime priority there. On the other hand, the power distribution within the domain governs most of the aging and drift effects, as well as those in the HAZ. An interpretation of the global, average power conversion is not qualified to describe them. The local power density can be calculated by

$$\varrho(x,y) = z\kappa(\nabla\varphi(x,y))^2 \text{ on } \Omega\backslash\Gamma \quad (5)$$

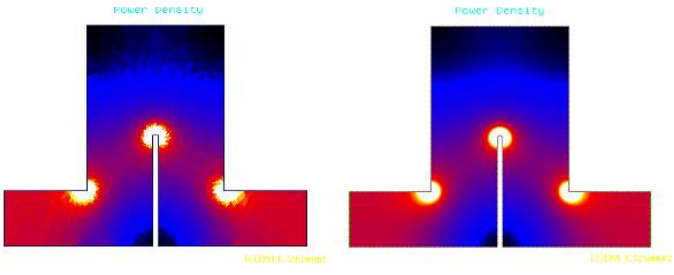

Fig. 5. Power density distribution of a shape similar to Fig. 4 (*left*: FEM-solution; *right*: BEM-solution)

By using first derivatives of the fundamental solutions in the formula for interior points of the BEM the gradient can be calculated with a high resolution. This results in smooth and reliable power distribution maps (Fig. 5). Again, an important benefit of the BEM for the model of section II where the power density distribution in the HAZ is to explore.

V. Examples

Iteration of (3) changes domain geometry $\Omega(t_j)$ for each time step and the higher the local power density the faster the boundary section will move. Fig. 6 presents this virtual effect of a trimmed bar resistor structure whereby the heat affected zone width is selected to be unreal large for a better view (surrounding dotted lines).

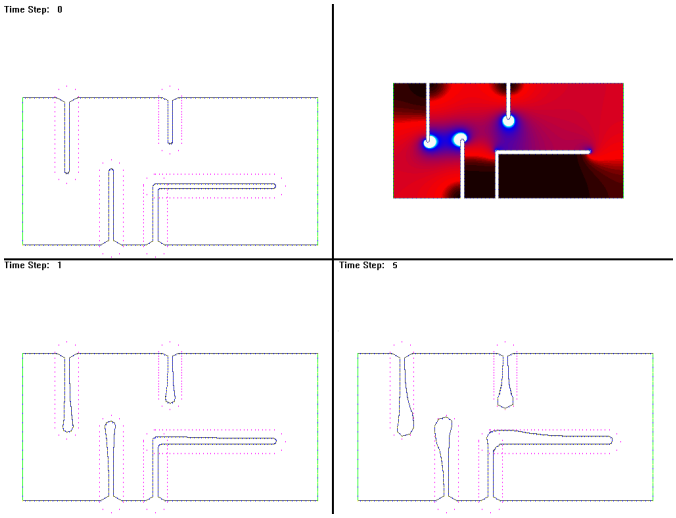

Fig. 6. Virtual HAZ edge degeneration of a trimmed bar resistor; the terminals are at left and right hand side (*top left*: initial situation; *top right*: initial power density map; *lower left*: degeneration after one time step and after 5 time steps *lower right image*)

A more realistic example gives Fig. 7. The designer may have the choice between the four shown trim pathways of a bar resistor. All of them have the same final resistance.

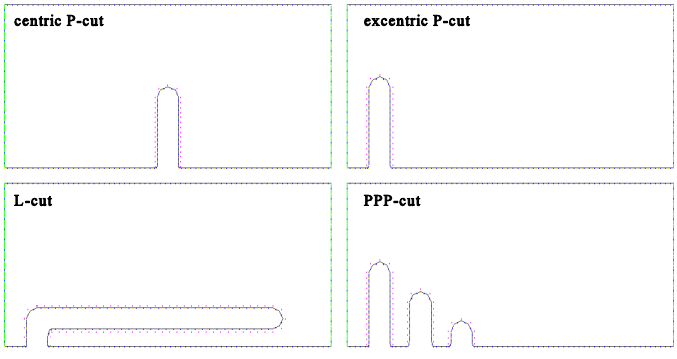

Fig. 7. Four different trim figure proposals for the same bar resistor layout and the same final resistance (the terminals are always at right and left hand side)

The model of section II plots a discrete view graph of post-trim drift versus time by resistance computation for each time step t_j. The result of the four samples is presented in Fig. 8. The function $r(t)$ expresses the ratio of the absolute resistance $R(t)$ to the inital resistance at time $t_0 = 0$.

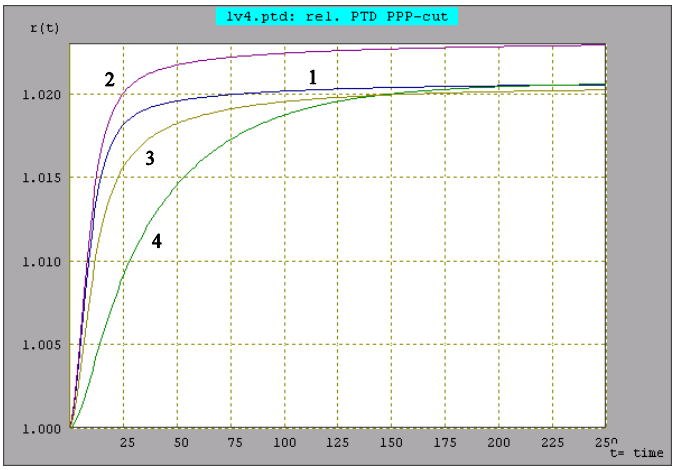

Fig. 8. Dynamic post-trim drift characteristics of Fig. 7 bar resistors (1: excentric P-cut; 2: centric P-cut; 3: PPP-cut; 4: L-cut; [t]= h)

The view graphs reveal that each trim figure behave differently. The highest final post-trim drift is expectable for the centric P-cut and the lowest one for the PPP-cut. Further, it can be seen that the L-cut has the lowest drift velocity and the excentric P-cut drifts faster than all the other. Only the single P-cuts deliver simple trim strategies. But they have mostly a too worse trim sensitivity for a high precision result. If a more complex trim strategy is affordable, the designer can now chose the PPP-cut for the shortest burn-in process. Such evaluations at design stage without real world experiments weren't possible before. But for a comparative assessment only, the dynamical post-trim drift model is useable with more or less fictive parameters, too.

VI. Conclusion

The usefullness of the BEM as a fast, precise and robust method is shown for the computation of film resistor's post-trim drift behavior. It is also shown that other well known methods, like FEM, are less suitable to model the phenomenon of post-trim drift. Resistor precision requirements in IC production increase permanently, and so also the necessity to choose proper trim pathways. These computations deliver additional, fundamental selection criterions for designers and hereby are of future importance.

References

[1] K. Schimmanz, *Konzipieren und Bewerten von Hochpräzisions-Hybridwiderständen durch Laser-Trimm-Simulation*, Dr.-Ing. thesis, TU-Berlin, 2002.

[2] A. Kost, *Numerische Methoden in der Berechnung elektromagnetischer Felder*, Springer Verlag, Berlin, 1994.